Dissociative and nondissociative photoionization of H_2 from the $E,F^1\Sigma_g^+$ excited state

Jorge Fernández* and Fernando Martín†
Departamento de Química C-9, Universidad Autónoma de Madrid, 28049 Madrid, Spain
(Received 7 December 2006; published 23 April 2007)

We present a theoretical study of dissociative and nondissociative photoionization of H_2 from the $E,F^1\Sigma_g^+(v,J=0)$ excited state for $v=0-9$ in the photon energy range 3 to 14 eV. We have found that, for most initial v's, dissociative ionization is the dominant process for photon energies well above the dissociative ionization threshold. In this photon energy range, resonance structures arising from autoionization of the Q_1 doubly excited states of H_2 are observed. Cross sections differential in the energy of the remaining H_2^+ ion or in the proton kinetic energy are analyzed in detail for a photon energy of 6.4 eV corresponding to the wavelength of an ArF excimer laser. Comparison of our results with the available experimental measurements is good. We show, however, that contribution of the Q_1 doubly excited states to the measured dissociative ionization cross section is more important than originally believed.

DOI: 10.1103/PhysRevA.75.042712 PACS number(s): 33.80.Eh, 33.80.Rv, 33.60.−q, 33.80.−b

I. INTRODUCTION

Molecular photoionization is a process in which the excess photon energy is shared by both electrons and nuclei. Thus the outgoing electron can absorb part of the available energy leading either to a residual molecular ion in a particular vibrational state (nondissociative photoionization) or to dissociation into smaller molecular and/or atomic fragments (dissociative photoionization). Both processes have been extensively investigated in the simplest molecule, H_2, in particular ionization produced by absorption of a single xuv photon from the ground $X^1\Sigma_g^+(v=0)$ state (see, e.g., a recent review on the subject [1]). In this case, dissociative photoionization leading to $H+H^+$ is less than 10% of the total cross section. In spite of this, when the photon energy is large enough to populate doubly excited states, the dissociative photoionization spectra exhibit resonant peaks in the kinetic energy distribution (KED) of ejected protons [2–5]. As a consequence of the coupling between resonant and nonresonant processes, and the interference with the nuclear motion, the peaks exhibit complex forms and, very often, are difficult to assign [6,7]. Interestingly, there is almost no trace of resonant effects in the photoelectron energy spectra or in the vibrational energy distribution of H_2^+ ions formed in the nondissociative process (see [1]).

The introduction of moderately intense laser sources have made it possible to populate high lying electronic states of H_2 via multiphoton excitation [8]. From these states, ionization and dissociation can be produced with less energetic photons. Most experiments have concentrated on the $E,F^1\Sigma_g^+$ state [9–13], which is usually populated by absorption of two identical photons. A subsequent photon can then excite the molecule above the ionization limit and lead to both dissociative and nondissociative photoionization (see Fig. 1). The global process is called (2+1) resonant enhanced multiphoton ionization (REMPI). This process occurs for a photon energy of about 6.4 eV. Pioneering experiments of Anderson *et al.* [9] showed that (2+1) REMPI of H_2 through the $E,F^1\Sigma_g^+$ intermediate state leads to a non-Franck-Condon vibrational distribution of the remaining H_2^+ ion. Both this vibrational distribution and the photoelectron angular distribution associated with individual H_2^+ vibrational states were shown to vary significantly with the specific vibrational state that is resonantly populated by absorption of the first two photons. These findings were theoretically interpreted in the late 1980s by Rudolph *et al.* [14] and Cornaggia *et al.* [15] using, respectively, the Hartree-Fock frozen core approximation and the multichannel quantum defect theory to describe the molecular continua [15].

In later (2+1) REMPI experiments using 6.4 eV photons, the dissociative ionization channel has also been investigated. In particular, Xu *et al.* [10] and Hill and co-workers [11,12] have shown that, similarly to ground state H_2 photoionization, nondissociative photoionization produced by absorption of the third photon from the $E,F^1\Sigma_g^+$ state is the dominant process. Xu *et al.* [10] have obtained in addition the detailed H_2^+ vibrational distribution corresponding to H_2 photoionization from different $E,F^1\Sigma_g^+(v)$ vibronic states. More recently, Bakker *et al.* [13] have measured the KED and the angular distribution of protons produced in one-photon dissociative ionization from the $E,F^1\Sigma_g^+(v=6,J=0)$ state using again 6.4 eV photons. The latter measurements have revealed pronounced oscillations in the proton KED, which has been interpreted as the signature of direct (i.e., nonresonant) dissociative ionization.

Simple theoretical models have been used to interpret the latter findings in the dissociative ionization channel. For instance, the interferences between different ionization and dissociation channels were either treated approximately [10] or neglected [13]. Although these model calculations have been very useful to uncover the basic mechanisms behind the experimental observations, there still remain quantitative discrepancies that should be investigated using fully *ab initio* methods. Furthermore, apart from the work of Ref. [10], in which different vibrational levels of the $E,F^1\Sigma_g^+$ state have been considered, the most recent experiment to date have concentrated on the $E,F^1\Sigma_g^+(v=6,J=0)$ initial state, which is

*Electronic address: j.fernandez@uam.es
†Electronic address: fernando.martin@uam.es; URL: http://www.uam.es/quimica/spline

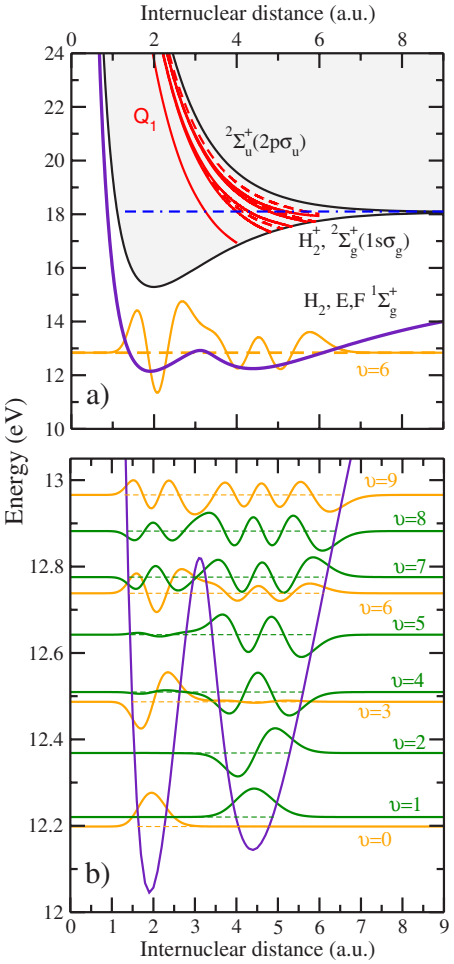

FIG. 1. (Color online) (a) Potential energy curves of H_2 relevant for the (2+1) REMPI process described in the text. The potential energy curve of the $E,F^1\Sigma_g^+$ state is taken from Ref. [16]. Red lines: Q_1 $^1\Sigma_g^+$ doubly excited states; red dashed lines: Q_1 $^1\Pi_u$ doubly excited states [17]. The energy origin is placed on the lowest rovibrational level of the ground electronic state of H_2. The figure shows a typical vibrational wave function in the $E,F^1\Sigma_g^+$ electronic state (v=6). (b) Vibrational energies and wave functions associated with the $E,F^1\Sigma_g^+$ state.

directly populated from the ground state via a vertical transition. Thus, it is not clear if oscillations as those reported in Ref. [13] for the proton KED also exist for other initial vibrational states. Furthermore, we do not know if the above findings change with the energy of the ionizing photon, since all experiments were performed at a fixed wavelength of approximately 190 nm (6.4 eV) corresponding to the ArF excimer laser. Varying the energy of the ionizing photon might be achieved in two-color (2+1) photoionization experiments by using an additional tunable laser. To investigate these problems we have performed fully *ab initio* calculations of dissociative and nondissociative photoionization of H_2 from the $E,F^1\Sigma_g^+(v,J=0)$ excited state for v=0–9 in the photon energy range 3–14 eV. The theoretical method is the same as that successfully used to study dissociative ionization of H_2 from the ground state [6,7,18].

II. THEORY

The theoretical method has been described in detail elsewhere [18]. Briefly, the photoionization cross section is evaluated in the dipole approximation

$$\sigma_{\alpha v_\alpha}(E) = \frac{4\pi^2\omega}{3c}\sum_{pl_\alpha m}\left|\int dR\langle\Psi_{iv}|\vec{e}_p\cdot\vec{D}|\Psi^+_{\alpha v_\alpha El_\alpha m}\rangle\right|^2, \quad (1)$$

where α indicates the electronic state of the residual ion and v_α the corresponding vibrational (or dissociative) state, l_α is the angular momentum of the ionized electron, m is the corresponding azimuthal quantum number, $\Psi_{iv}(\mathbf{r},R)$ is the initial $E,F^1\Sigma_g^+(v)$ state, $\Psi^+_{\alpha v_\alpha El_\alpha m}(\mathbf{r},R)$ is the final state, $\mathbf{r}$ represents the electronic coordinates, R is the internuclear distance, $\vec{D}$ is the two-electron dipole operator, and $\vec{e}_p$ is the photon polarization vector. The energy E is given by $E=W_{iv}+\hbar\omega$, where W_{iv} is the total energy of the molecule in the initial state and $\hbar\omega$ is the photon energy. The wave functions Ψ_{iv} and $\Psi^+_{\alpha v_\alpha El_\alpha m}$ are evaluated in the adiabatic approximation as described in Ref. [18]. The final state wave function $\Psi^+_{\alpha v_\alpha El_\alpha m}$ is not simply given by the product of an electronic and a nuclear wave function. It results from a close-coupling calculation that accounts for interferences among the various electronic and nuclear channels:

$$\Psi^+_{\alpha v_\alpha El_\alpha}(\mathbf{r},R) = \sum_{r'}\phi_{r'}(\mathbf{r},R)\xi^{r'}_{\alpha v_\alpha l_\alpha E}(R) + \psi^{0+}_{\alpha l_\alpha\epsilon_\alpha}(\mathbf{r},R)\chi_{v_\alpha}(R)$$
$$+\lim_{\eta\to0}\sum_{r'}\sum_{\alpha' l'_{\alpha'}}\sum_{v'_{\alpha'}}\int\!\!\!\!\!\!\int dE'\frac{1}{E-E'+i\eta}$$
$$\times\int dR' V^{r'*}_{\alpha' v'_{\alpha'} l'_{\alpha'} E'}(R')\xi^{r'}_{\alpha v_\alpha l_\alpha E}(R')$$
$$\times\psi^{0+}_{\alpha' l'_{\alpha'}\epsilon'_{\alpha'}}(\mathbf{r},R)\chi_{v_{\alpha'}}(R), \quad (2)$$

where

$$V^r_{\alpha v_\alpha l_\alpha E}(R) = \langle\phi_r|H_{\rm el}|\psi^{0+}_{\alpha l_\alpha\epsilon_\alpha}\rangle\chi_{v_\alpha}(R), \quad (3)$$

$H_{\rm el}$ is the electronic Hamiltonian, ϵ_α is the kinetic energy of the outgoing electron in channel α, $\phi_r(\mathbf{r},R)$ is a resonant electronic state of energy $E_r(R)$, and $\psi^{0+}_{\alpha l_\alpha\epsilon_\alpha}(\mathbf{r},R)$ represents the nonresonant electronic continuum in which the former are embedded. Note that we have dropped the index m because $^1\Sigma_g^+$ and $^1\Pi_u$ continuum states, which have different m, are not coupled. In Eqs. (2) and (3), χ_{v_α} is a nuclear wave function that describes the motion of the nuclei in the α state of H_2^+, and $\xi^r_{\alpha v_\alpha l_\alpha E}$ is the solution of

$$[E-E_r(R)-T(R)]\xi^r_{\alpha v_\alpha l_\alpha E}(R)$$
$$= V^r_{\alpha v_\alpha l_\alpha E}(R) + \lim_{\eta\to0}\sum_{r'}\sum_{\alpha' l'_{\alpha'}}\sum_{v'_{\alpha'}}\int\!\!\!\!\!\!\int dE'\frac{V^r_{\alpha' v'_{\alpha'} l'_{\alpha'} E'}(R)}{E-E'+i\eta}$$
$$\times\int dR' V^{r'*}_{\alpha' v'_{\alpha'} l'_{\alpha'} E'}(R')\xi^{r'}_{\alpha v_\alpha l_\alpha E}(R'). \quad (4)$$

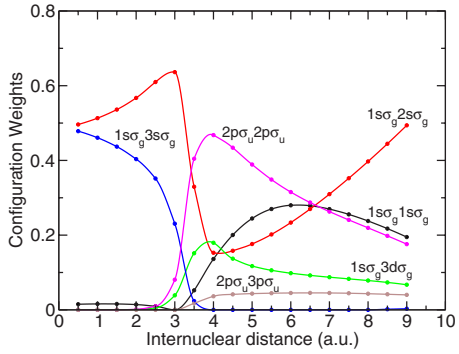

FIG. 2. (Color online) Configuration weights for the $E,F^1\Sigma_g^+$ state.

The latter equation represents the nuclear motion when the electrons are in the quasistationary state ϕ_r. The matrix element in Eq. (3) represents the coupling between the resonance ϕ_r and the nonresonant wave function $\psi^{0+}_{\alpha l_\alpha \epsilon_\alpha}$ and vibrational state χ_{v_α} (the modulus square of the bracket is proportional to the corresponding autoionization width). Hence, the two terms in the right-hand side of Eq. (4) are the result of the autoionizing character of the ϕ_r state.

All electronic wave functions are represented by linear combinations of two-electron configurations built from one-electron molecular orbitals represented in a basis of B-spline functions [19] of order 8 in a box of 60 a.u. Bound molecular orbitals include angular momenta up to $l_{\max}=26$ and 200 B-splines per l. Orbitals associated with a continuum electron include angular momentum up to $l=8$. The nuclear wave functions are represented in a basis of 280 B splines of order eight defined in a box of 18 a.u.

The initial $E,F^1\Sigma_g^+$ state of H_2 has been evaluated in a basis of two-electron configurations built from B-spline representations of Slater-type orbitals (STOs) and molecular orbitals (MO). Configurations involving STOs have been built as described in Ref. [1]. Configurations involving MOs are $n_1\sigma_g n_2\sigma_g(n_1=1-5,n_2=1-25)$, $n_1\sigma_u n_2\sigma_u(n_1=1-5,n_2=1-25)$, $n_1\pi_g n_2\pi_g(n_1=1-4,n_2=1-20)$, $n_1\pi_u n_2\pi_u(n_1=1-4,n_2=1-20)$, $n_1\delta_g n_2\delta_g(n_1=1-3,n_2=1-15)$, and $n_1\delta_u n_2\delta_u(n_1=1-3,n_2=1-15)$. This amounts to 840 configurations. This basis gives an energy for the ground state at the equilibrium distance ($R=1.4$ a.u.) of −1.171975 a.u., which is 0.002 a.u. higher than the best known value [20]. For the $E,F^1\Sigma_g^+$ excited state, we have obtained an energy of −1.243852 a.u. at the first minimum ($R=1.9$ a.u., see Fig. 1) −1.011379 a.u. at the maximum ($R=3.1$ a.u.), and −0.936852 a.u. at the second minimum ($R=4.4$ a.u.), which are 0.0006, 0.0009, and 0.0049 a.u. higher, respectively, than the accurate values of Ref. [16]. We show in Fig. 2 the main configurations that characterize the $E,F^1\Sigma_g^+$ state. As can be seen, this state is not described by a dominant type of configuration, in contrast with the ground state. This implies that, as pointed out in previous works, qualitatively assignment of possible transitions in terms of a single configuration picture is much more difficult and probably ambiguous.

The resonant wave functions ϕ_r have been obtained by diagonalizing the H_2 Hamiltonian in a basis of ≃200 configurations built from B-spline representations of MOs as described in Refs. [17,21]. Here we have only considered the lowest six states of the Q_1 series with symmetries $^1\Sigma_u^+$ and $^1\Pi_u$. These states have the largest autoionization widths [17]. Resonant states belonging to the Q_2 and higher series are not relevant except at the higher photon energies considered in this work (14 eV). The Q_1 states lie above the ionization threshold at short and intermediate R (see Fig. 1). At $R=R_c$, their energies cross the ionization threshold and the states lose their autoionizing character. As R increases, the resonant states cross the $1s\sigma_g nl\lambda$ Rydberg series and dissociate into $H(1s)+H(n>1)$.

The nonresonant wave functions $\psi^{0+}_{\alpha l_\alpha \epsilon_\alpha}$ describe a bound electron in either the $1s\sigma_g$ or $2p\sigma_u$ orbitals of H_2^+ and a continuum electron. They have been obtained with the L^2 close-coupling method [1]. The method consists in evaluating the electronic continuum Green's function in the discrete basis of two-electron configurations built from the B-spline representations orbitals mentioned above. The use of a discrete basis implies that the Green's function is obtained from the solution of a system of algebraic equations that it is much easier to solve than the original integrodifferential equation associated with a true electronic continuum. It is important to note that the L^2 close-coupling method allows for interchannel coupling between different open channels and partial waves, and yields the correct outgoing asymptotic behavior (see Ref. [18] for details).

III. IONIZATION WITH 6.4 eV PHOTONS

We first present a detailed study at a fixed photon energy of 6.4 eV, which is around the value used in all previously reported experiments. In the next section we will analyze the variation with photon energy.

A. Nondissociative photoionization

Figure 3 shows the vibrational distribution of H_2^+ molecular ions formed in photoionization of H_2 from the $E,F^1\Sigma_g^+(v,J=0)$ electronic state for $v=0-9$ and a photon energy of 6.4 eV. The final $H_2^+(v)$ vibrational distributions strongly depend on the initial vibrational level v. For $v=0$, 3, and 6, H_2^+ remains in low vibrational states, while for $v=1$, 2, and 4, it remains in highly excited vibrational states. For other initial values of v, H_2^+ is produced in both low and high vibrational states. This complicated behavior is the consequence of the two potential wells in the $E,F^1\Sigma_g^+$ state: initial vibrational states mainly localized around the inner well lead to low-v H_2^+ distributions while initial vibrational states mainly localized around the outer well lead to high-v H_2^+ distributions due to the more favorable Franck-Condon overlap. Those vibrational states with no clear localization lead to much broader $H_2^+(v)$ distributions. Figure 3 also shows the contribution from the nonresonant part of the final continuum state [second term in the right hand side of Eq. (2)]. It can be seen that, in the case of initial vibrational states clearly localized around the inner minimum ($v=0$ and 3), most of the calculated intensity comes from the nonresonant term, while the opposite is observed for other initial vibrational states. The fact that, for $v=0$, the total cross section is

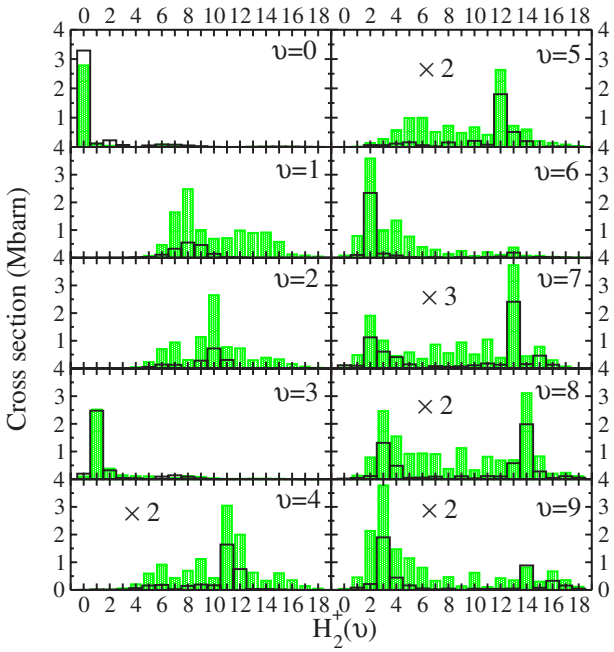

FIG. 3. (Color online) Final H_2^+ vibrational distribution in H_2 photoionization from the $E,F^1\Sigma_g^+(\upsilon)$ for $\upsilon=0-9$ and a photon energy of 6.4 eV. Full bars: total cross section; hollow bars: nonresonant contribution.

smaller than the nonresonant cross section is due to the interference between the resonant and nonresonant terms. As we will see below, the same occurs in the case of dissociative ionization.

Figure 4 shows the contribution of the final H_2 $^1\Sigma_u^+$ and $^1\Pi_u$ symmetries to the above vibrational distributions. For

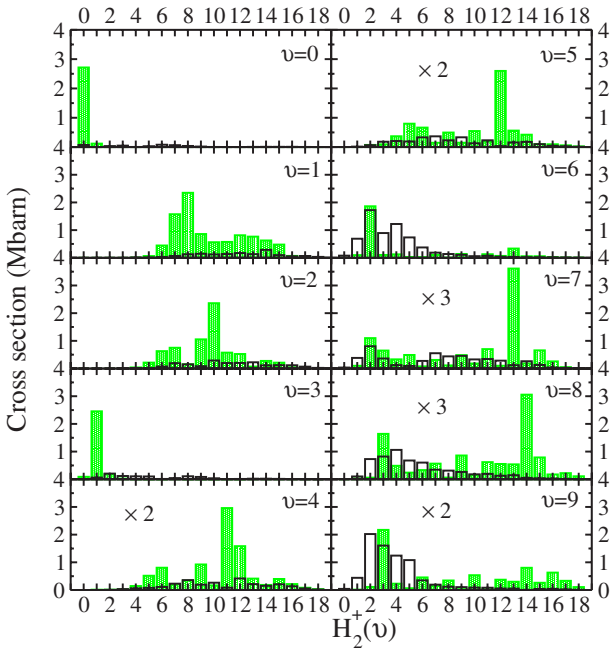

FIG. 4. (Color online) $^1\Sigma_u^+$ and $^1\Pi_u$ contributions to the H_2^+ vibrational distribution in H_2 photoionization from the $E,F^1\Sigma_g^+(\upsilon)$ for $\upsilon=0-9$ and a photon energy of 6.4 eV. Full bars: $^1\Sigma_u^+$ contribution; hollow bars: $^1\Pi_u$ contribution.

most initial values of υ, the largest contributions come from the $^1\Sigma_u^+$ symmetry. Also $H_2^+(\upsilon)$ vibrational distributions associated with the $^1\Sigma_u^+$ symmetry are in general much broader (i.e., less Franck-Condon) than those arising from the $^1\Pi_u$ one. This broadening is due to the resonant contribution of the Q_1 states of $^1\Sigma_u^+$ symmetry, which are much more efficiently populated than those of $^1\Pi_u$ symmetry.

Our results are compared in Fig. 5 with the experimental measurements reported in Ref. [10]. Very good agreement is obtained up to $\upsilon=6$. For $\upsilon=9$, the absolute values for high υ are smaller than those for small υ, while they are comparable in the experiment. Nevertheless the relative intensities in both regions taken separately are in qualitative agreement with experiment. It is worth pointing out that, except for the latter case, the present results (either convoluted or unconvoluted) agree better with experiment than those obtained in early theoretical work [14] or from the simple model reported in Ref. [10]. For instance, for $\upsilon=6$, the experiment and the present theoretical calculations predict a decrease of intensity from $\upsilon'=2$ to $\upsilon'=3$ and then an increase up to $\upsilon'=4$, while the previous theoretical results [10,14] predict a monotonous decrease in this region. The multichannel quantum defect calculations reported in Refs. [14,15] for $\upsilon=0$ and 3 are in reasonable agreement with ours.

B. Dissociative photoionization

Figure 6 shows the KED of protons produced in dissociative photoionization of H_2 from the $E,F^1\Sigma_g^+(\upsilon,J=0)$ state for $\upsilon=0-9$ and a photon energy of 6.4 eV. Notice that the maximum allowed kinetic energy for ejected protons is given by $T_{\max}=(\hbar\omega-E_{\text{th}})/2$, where E_{th} is the threshold energy for dissociative photoionization from a given $E,F^1\Sigma_g^+(\upsilon,J=0)$ initial state. Thus the theoretical cross sections go abruptly to zero for $T=T_{\max}$. As for nondissociative photoionization, the present results strongly depend on the initial vibrational level υ. For $\upsilon=0$, 3, and 6, dissociative photoionization is much less important than for other initial values of υ: the calculated cross sections are more than an order of magnitude smaller (notice that, for a better visualization, in Fig. 6 the corresponding cross sections have been multiplied by 50, 60, and 8, respectively). Consequently, the ratio of dissociative vs nondissociative ionization is smaller for $\upsilon=0$, 3, and 6 (see Fig. 10 below). Therefore, for these initial states, experimental determination of the dissociative ionization cross section is most difficult. As mentioned above, these are the initial vibrational states localized around the inner well which favor the production of H_2^+ in a low vibrational state. For vibrational states localized around the outer well, the higher H_2^+ vibrational states, in particular those associated with the vibrational continuum, are favored. This also explains why, for $\upsilon\neq 0$, 3, and 6, the ratio of dissociative vs nondissociative ionization is significantly larger than in photoionization from the ground $X\ ^1\Sigma_g^+$ state. Figure 6 also shows the contribution from the nonresonant part of the final continuum state [second term in the right-hand side of Eq. (2)]. It can be seen that, except for $\upsilon=1$, resonance effects induced by the Q_1 doubly excited states are not dominant, but are not negligible. For $\upsilon=1$, a direct vertical transition from the outer

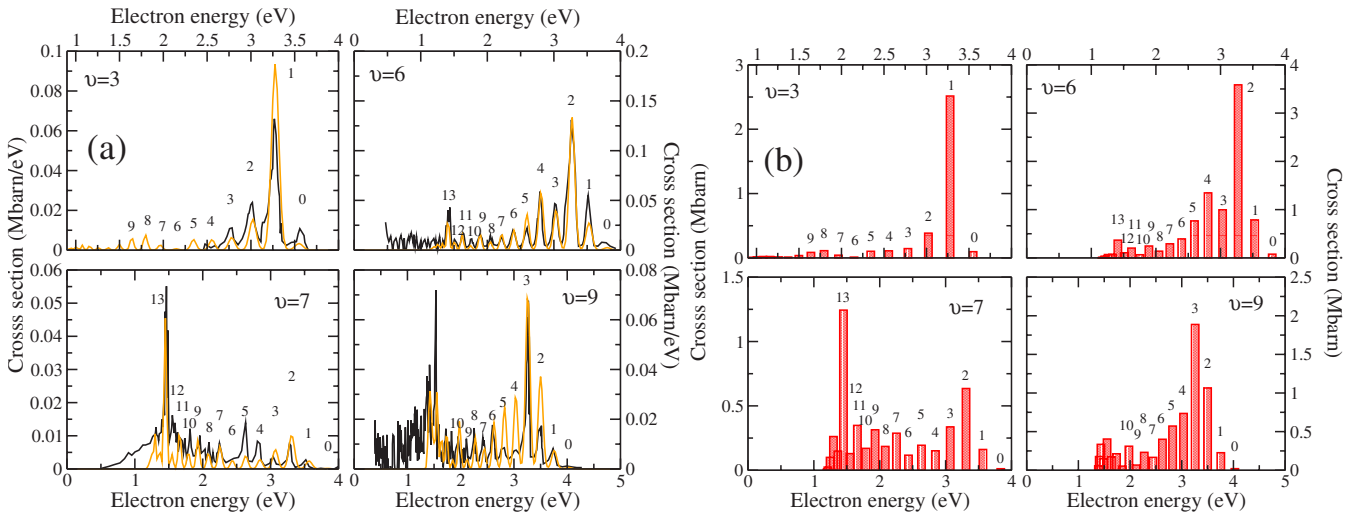

FIG. 5. (Color online) (a) Comparison between calculated (orange) and measured (black, Ref. [10]) H_2^+ vibrational distribution in H_2 photoionization from the $E,F^1\Sigma_g^+(v)$ state for v=3, 6, 7, and 9, and a photon energy of 6.4 eV. To account for the limited energy resolution of the experiment, the theoretical results have been convoluted to a Gaussian with FWHM of 3% of the electron energy. (b) Theoretical distributions without convolution.

minimum to the second $Q_1\ ^1\Sigma_u^+$ doubly excited state is possible. For $v \geqslant 9$, the vibrational wave function resembles that of a common single-well electronic state, so that excitation to the doubly excited states follows the more traditional behavior based on vertical transitions from the outer classical turning point.

An interesting feature of the KEDs presented in Fig. 6 is the existence of pronounced oscillations. These oscillations are present in both the resonant and nonresonant contributions. Figure 7(a) shows the contribution of the $1s\sigma_g$ and $2p\sigma_u$ ionization channels. The oscillatory behavior is observed in both channels. By comparing Figs. 6 and 7(a), it can be seen that the resonant contribution is very similar to the $1s\sigma_g$ cross section and the nonresonant contribution to the $2p\sigma_u$ cross section. This confirms that resonance effects are mostly due to the Q_1 doubly excited states lying below the $^2\Sigma_u^+(2p\sigma_u)$ ionization threshold. The oscillations in the $2p\sigma_u$ channel are a direct consequence of the variation of the Franck-Condon overlap between the initial vibrational state and the dissociative states associated with the $2p\sigma_u$ channel (see Ref. [13]). The Franck-Condon factors also explain why the frequency of the oscillations increases with the initial vibrational quantum number v. Figure 7(b) shows the contribution of the final $H_2\ ^1\Sigma_u^+$ and $^1\Pi_u$ symmetries to the KEDs. It can be seen that $^1\Sigma_u^+$ and $^1\Pi_u$ contributions are comparable. For $v \geqslant 5$, the oscillatory behavior is observed for both symmetries, although it is somewhat distorted in the $^1\Sigma_u^+$ contribution for v=6 due to the significant contribution of the Q_1 doubly excited states.

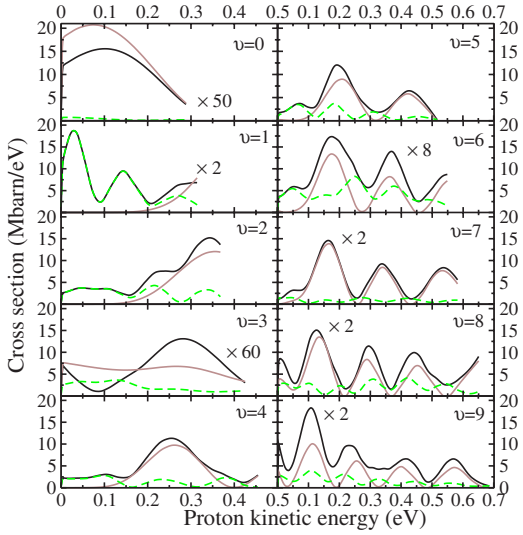

FIG. 6. (Color online) Proton kinetic energy distribution in H_2 photoionization from the $E,F^1\Sigma_g^+(v)$ state for v=0–9 and a photon energy of 6.4 eV. Full black lines: dissociative ionization cross section; full brown lines: nonresonant contribution; dashed green lines: resonant contribution.

In Fig. 8 we compare the calculated spectra from the initial $E,F^1\Sigma_g(v=6)$, state with the available experimental results [13]. These measurements correspond to protons observed over all angles with respect to the polarization vector of the incident radiation. Since the measurements are not given in an absolute scale, the experimental data have been normalized to the calculated cross section for a proton kinetic energy of 0.17 eV. It must be stressed again that comparisons for the initial $E,F^1\Sigma_g(v=6)$, state are much more difficult than for other initial values of v because, as shown in Fig. 6, the corresponding cross section is one of the smallest ones (remember that this is the consequence of the initial v=6 vibrational state having the larger maxima in the inner well). In spite of this, the theory reproduces most of the features observed in the experiment: peaks A (0.17 eV), B (0.37 eV), and C (0.57 eV), their shape, and relative intensities (our results slightly overestimate the intensity of peak B). Convolution of the theoretical results with the apparatus function leads to a better agreement with experiment for peaks A and B, but worse for peak C. The origin of the

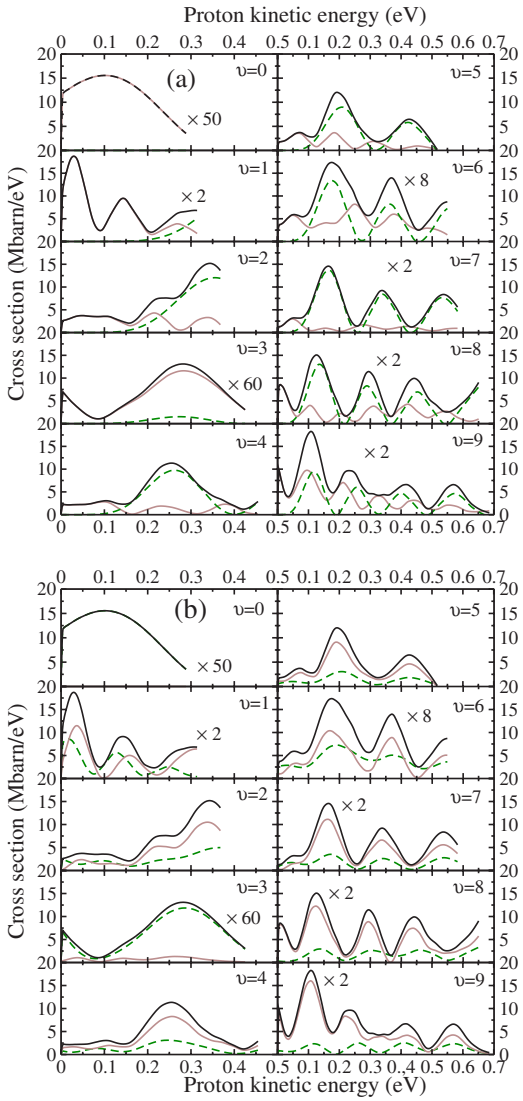

FIG. 7. (Color online) Contribution of (a) the $1s\sigma_g$ (full brown lines) and $2p\sigma_u$ (dashed green lines) channels and (b) the $^1\Sigma_u^+$ (dashed green lines) and $^1\Pi_u$ (full brown lines) symmetries to the proton kinetic energy distribution (full black lines) in H_2 photoionization from the $E,F\,^1\Sigma_g^+(\upsilon)$ for υ=0–9 and a photon energy of 6.4 eV.

disagreement for peak C might be the use of the adiabatic approximation since this peak is associated with emission of very slow electrons for which nonadiabatic effects might play a significant role. As shown in Fig. 6, for the initial υ =6 state, these peaks are present in both the resonant and nonresonant contributions. In Ref. [13], all these structures were exclusively attributed to nonresonant dissociation though the $^2\Sigma_u^+(2p\sigma_u)$ channel. Although, as we have seen, this is approximately true for most initial υ's, contribution of the $Q_1\ ^1\Sigma_u^+$ doubly excited states is relatively more important for υ=6.

Using a semiclassical model, we can relate the position of each resonant peak with the internuclear distance R_i at which autoionization is produced by using the formula [4,7]

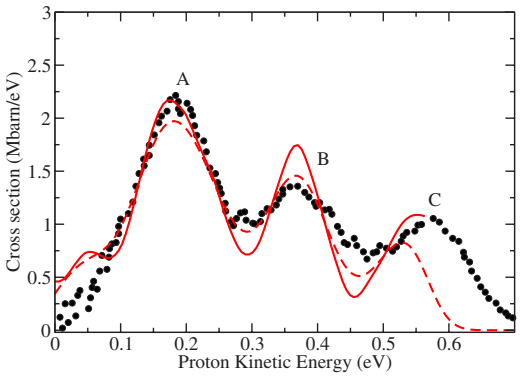

FIG. 8. (Color online) Comparison between the calculated (full line) and measured (circles, Ref. [13]) proton kinetic energy distribution in H_2 photoionization from the $E,F\,^1\Sigma_g^+(\upsilon=6)$ state and a photon energy of 6.4 eV. The dashed line shows the convolution of the theoretical curve to a Gaussian function with FWHM of 0.05 eV; this is the experimental energy resolution at the highest proton kinetic energy.

$$2T_i = \hbar\omega + W_{i\upsilon} - E_{H_{1s}} - [E_r(R_i) - E_\alpha(R_i)], \tag{5}$$

where T_i and $[E_r(R_i)-E_\alpha(R_i)]$ are the kinetic energies of the ejected proton and electron, respectively, $E_{H_{1s}}$ is the ground-state energy of the H atom, and $W_{i\upsilon}-E_{H_{1s}} \simeq 5.24$ eV. For the lowest $Q_1\ ^1\Sigma_u^+$ resonant state, we obtain $R>3.5$ a.u. in the relevant range of T_i. This means that autoionization occurs immediately before the doubly excited state crosses the first ionization limit (see Fig. 1). This is consistent with the fact that the corresponding autoionization width increases with internuclear distance (see Ref. [17]). Contributions from the $Q_1\ ^1\Pi_u$ doubly excited states are much smaller due to the smaller autoionization widths (see Ref. [17]).

We now analyze the angular distribution of ejected protons. The differential cross section for proton emission in the solid angle $\Omega_{k_{H^+}}$ along the direction k_{H^+} of the ionic fragments is given by

$$\frac{d\sigma_{\alpha\upsilon_\alpha}}{dEd\Omega_{k_{H^+}}} = \frac{\sigma_{\alpha\upsilon_\alpha}(E)}{4\pi}\left[1+\beta_{\alpha\upsilon_\alpha}(E)\left(\frac{3\cos^2\theta_{k_{H^+}}-1}{2}\right)\right], \tag{6}$$

where $\Omega_{k_{H^+}}$ is the angle between the ionic fragment momentum and the incident polarization direction and $\beta_{\alpha\upsilon_\alpha}(E)$ is the asymmetry parameter given by

$$\beta_{\alpha\upsilon_\alpha}(E) = 2\frac{D^2_{\alpha\upsilon_\alpha\Sigma}(E) - D^2_{\alpha\upsilon_\alpha\Pi}(E)}{D^2_{\alpha\upsilon_\alpha\Sigma}(E) + 2D^2_{\alpha\upsilon_\alpha\Pi}(E)}, \tag{7}$$

where $D^2_{\alpha\upsilon_\alpha S}(E)$ for $S=\Sigma$ or Π, is the sum of the square of the matrix elements for each partial wave (see Ref. [22] for details). $\beta_{\alpha\upsilon_\alpha}(E)$ $[-1\leqslant\beta_{\alpha\upsilon_\alpha}(E)\leqslant 2]$ measures the relative importance of the parallel and perpendicular components of the electric dipole transition and characterizes the symmetry of the molecular state in the ionization continuum.

When the experimental results cannot distinguish between protons coming from different dissociation paths, one must

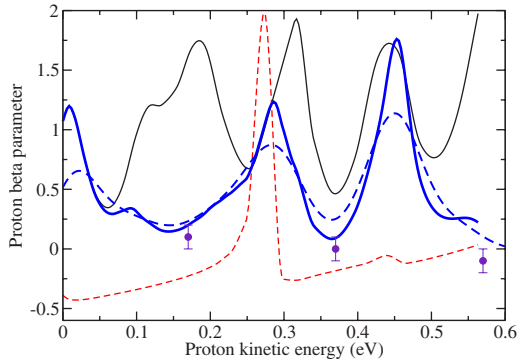

FIG. 9. (Color online) Asymmetry parameter at 6.4 eV photon energy. Thin full line: asymmetry parameter for protons dissociating through the $^2\Sigma_g^+(1s\sigma_g)$ ionic state; dashed line: asymmetry parameter for protons dissociating through the $^2\Sigma_u^+(2p\sigma_u)$ ionic state; thick full line: averaged asymmetry parameter; circles with error bars: experimental data from Ref. [13]. The thick dashed line shows the convolution of the theoretical curve to a Gaussian function with FWHM of 0.5 eV; this is the experimental energy resolution at the highest proton kinetic energy.

evaluate an average asymmetry parameter. For a photon energy of 6.4 eV, the accessible dissociation paths are those associated with the ground state and the first excited state of H_2^+, which are degenerate at infinite internuclear distance. In this case, the average asymmetry parameter is given by

$$\beta^A_{\alpha v_\alpha}(E) = \frac{\beta_{1s\sigma_g v_{1s\sigma_g}} \sigma_{1s\sigma_g v_{1s\sigma_g}} + \beta_{2p\sigma_u v_{2p\sigma_u}} \sigma_{2p\sigma_u v_{2p\sigma_u}}}{\sigma_{1s\sigma_g v_{1s\sigma_g}} + \sigma_{2p\sigma_u v_{2p\sigma_u}}}. \quad (8)$$

Figure 9 shows the calculated proton asymmetry parameter for dissociative ionization from the $E,F^1\Sigma_g^+(v=6)$ state of H_2 along the $^2\Sigma_g^+(1s\sigma_g)$ channel, the $^2\Sigma_u^+(2p\sigma_u)$ channel, and the average values resulting from Eq. (8). In the absence of the Q_1 $^1\Sigma_u^+$ doubly excited states, the value of $\beta_{1s\sigma_g}$ is close to zero in the whole range of proton kinetic energy. However, the $\beta_{1s\sigma_g}$ results shown in Fig. 9 clearly differ from this behavior, thus showing the importance of the Q_1 $^1\Sigma_u^+$ doubly excited states in the $^2\Sigma_g^+(1s\sigma_g)$ channel. The $\beta_{2p\sigma_u}$ parameter exhibits a sharp peak at 0.27 eV and a smaller peak at 0.45 eV, which are the consequence of the two minima in the $^2\Sigma_u^+(2p\sigma_u)$ partial cross section [see Fig. 7(a) for $v=6$]. As a consequence of the structures observed in the $\beta_{1s\sigma_g}$ and $\beta_{2p\sigma_u}$ parameters, the averaged asymmetry parameter $\beta^A_{\alpha v_\alpha}$ exhibits a nonmonotonous behavior. It can be seen that previous measurements of the average asymmetry parameter [13] agree reasonably well with the present calculations (a similar agreement is obtained when the theoretical results are convoluted with the apparatus function). The measurements were performed for proton kinetic energies in the vicinity of the calculated minima. In these minima, $\beta^A_{\alpha v_\alpha}$ is close to zero, but this is more the exception than the rule since $\beta^A_{\alpha v_\alpha}$ is always larger than zero and can reach values even close to the upper bound limit. It is worth noticing that in the absence of the Q_1 $^1\Sigma_u^+$ doubly excited states, $\beta^A_{\alpha v_\alpha} \simeq \beta_{2p\sigma_u}$ and the agreement with the experiment would worsen. In Ref. [13] it has been argued that a value of $\beta^A_{\alpha v_\alpha}$ close to zero indicates that the electron is mainly ejected in a d wave. However, an analysis of the different partial waves in the calculated wave function shows that contributions from the s wave are sometimes comparable to those from the d wave.

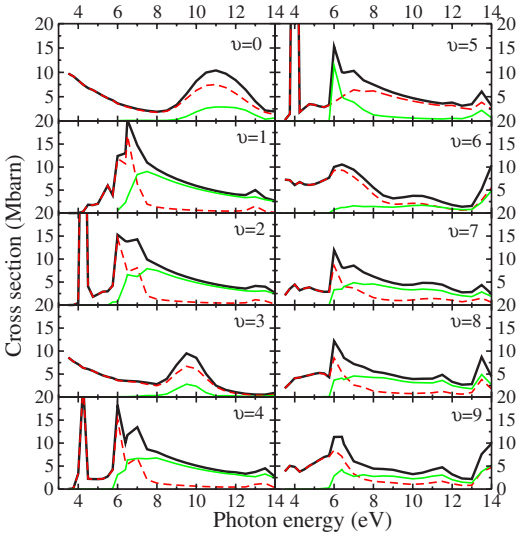

FIG. 10. (Color online) Photoionization cross section from the $E,F^1\Sigma_g^+(v)$ state of H_2 versus photon energy. Full thick line: total cross section; full thin line: dissociative photoionization cross section; dashed line: nondissociative photoionization cross section.

IV. VARIATIONS WITH PHOTON ENERGY

To obtain photoionization cross sections at energies as high as 14 eV, we have extended our calculations by also including the Q_2 doubly excited states of H_2. Although, as we will see below, these states play a minor role in most cases, there are a few exceptions at the higher photon energies. Figure 10 shows the variation with photon energy of the total photoionization cross sections from the $E,F^1\Sigma_g^+(v)$ state of H_2 for $v=0-9$. The relative contribution of dissociative and nondissociative processes is also shown. Dissociative ionization is only possible for photon energies larger than 5.9 eV [see Fig. 1(a)]. This threshold shifts to lower photon energies as v increases. The photon energy considered in the preceding sections (6.4 eV) lies very close to this threshold, especially for the higher v's. Close to this threshold, the nondissociative ionization process dominates for all initial v's and the ratio of dissociative vs nondissociative processes depends very much on this initial v. However, the situation changes completely when the photon energy is increased. Then the dissociative ionization process becomes dominant for most initial v's. This is in large contrast with H_2 photoionization from the ground X $^1\Sigma_g^+$ state for which the nondissociative cross section is always an order of magnitude larger than the dissociative one. The only exceptions are $v=0,3,5$, and to a lesser extent 6, but still the dissociative contribution is comparable to the nondissociative one at the higher photon energies (the reason why, in this case, the $v=5$ state follows

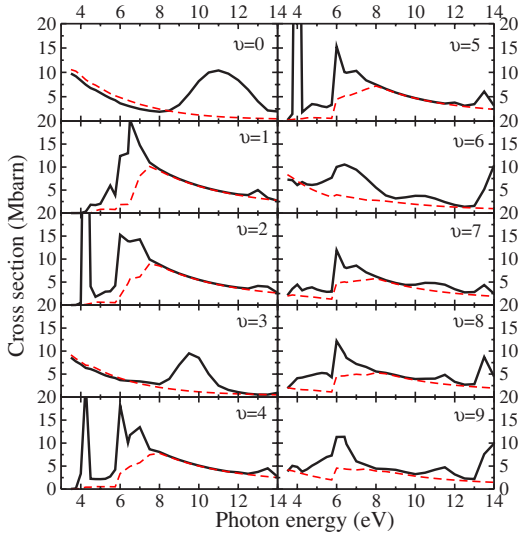

FIG. 11. (Color online) The same as Fig. 10 but now the dashed line represents the contribution of nonresonant ionization.

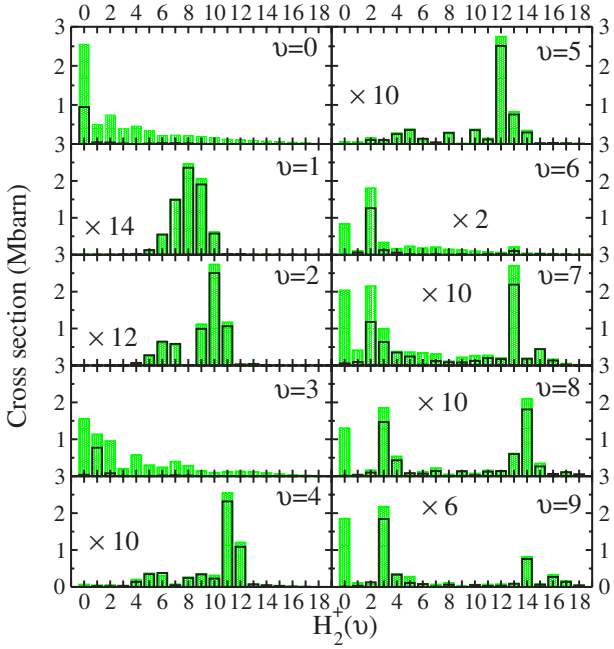

FIG. 12. (Color online) Final H_2^+ vibrational distribution in H_2 photoionization from the $E,F^1\Sigma_g^+(\upsilon)$ for $\upsilon=0-9$ and a photon energy of 10 eV. Full bars: total cross section; hollow bars: nonresonant contribution.

a behavior similar to that of the innerwell $\upsilon=0$, 3, and 6 states cannot be explained in terms of simple qualitative arguments).

Another interesting feature in Fig. 10 is the presence of peaks. The origin of these peaks can be understood by looking at Fig. 11, which shows the contribution of the nonresonant ionization process to the total cross section. It can be seen that the nonresonant ionization cross section varies smoothly with photon energy except in the vicinity of the dissociative ionization threshold. For $\upsilon=0$ and 3 (i.e., states with dominant innerwell vibrational maxima), there is a broad peak that dominates the photoionization spectrum. The origin of this peak is autoionization from the lowest $Q_1\ ^1\Sigma_u^+$ doubly excited states of H_2. Population of these states is possible through a vertical transition from the inner well of the initial $E,F^1\Sigma_g^+(\upsilon)$ state (see Fig. 1). The width of the peak corresponds more or less to the difference between the energy of the Q_1 state resulting from a vertical transition from the classical outer turning point and the energy of the Q_1 state resulting from a vertical transition from the classical inner turning point (both classical turning points are defined in the inner well). For the other initial υ's (i.e., those with important vibrational maxima in the outer well), the resonant peaks are much narrower and appear at much lower photon energy. These peaks are also associated with autoionization from the $Q_1\ ^1\Sigma_u^+$ doubly excited states, but since excitation is mainly produced from the outer well, they can be reached by using less energetic photons (see Fig. 1). Also, since these transitions take place in the region where the Q_1 doubly excited states cross the ionization threshold (below which they are no longer autoionizing states), the effective range of photon energies in which these states can autoionize is smaller. At variance with the $\upsilon=0$ and 3 cases, many $Q_1\ ^1\Sigma_u^+$ doubly excited states contribute to the peaks, especially for the higher υ's.

Figures 10 and 11 show that, for $\upsilon=6-9$, there are also resonant peaks at around 14 eV. These peaks are due to excitation to the lowest Q_2 doubly excited states through vertical transitions from the outer well of the $E,F^1\Sigma_g^+(\upsilon)$ state. For larger photon energies, more and more Q_2 doubly excited states will be populated. It is interesting to note that the Q_2 states are reached at much lower photon energies than in H_2 ground state photoionization, not only because excitation is produced from an excited electronic state but also because, for initial υ's with outer-well maxima, transitions occur at a large value of R (around 5 a.u.), a region where these doubly excited states are much lower in energy due to their dissociative character [see Ref. [7] and Fig. 1(a)].

Figures 12 and 13 show, respectively, the vibrational distribution of H_2^+ molecular ions and the KED of protons produced in photoionization of H_2 from the $E,F^1\Sigma_g^+(\upsilon,J=0)$ electronic state for $\upsilon=0-9$ and a photon energy of 10 eV. It can be seen that the results are very different from those shown in Figs. 3 and 6 for a photon energy of 6.4 eV. In the case of nondissociative photoionization, the largest cross sections are obtained for inner-well vibrational states $\upsilon=0$, 3, and 6, which have the largest Franck-Condon overlaps with the vibrational states of H_2^+. In contrast with the results obtained at 6.4 eV (Fig. 3), the cross sections for other initial υ's are much smaller at 10 eV. This is because, at variance with the 6.4 eV case, excitation from the outer-well vibrational states using a 10 eV photon does not lead to effective population of the Q_1 doubly excited states. This interpretation is confirmed by analyzing the contribution of the nonresonant process. Figure 12 shows that, for the outerwell vibrational states, the nonresonant contribution is almost identical to the complete result. It is only for the innerwell vibrational states that the resonant contribution is important, a result that is again in contrast with that obtained at 6.4 eV.

In the case of dissociative photoionization, initial outer-well states lead to oscillatory KED distributions (see Fig.

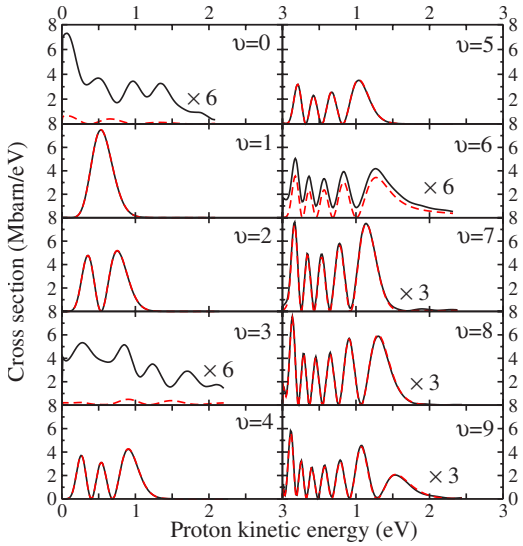

FIG. 13. (Color online) Proton kinetic energy distribution in H_2 photoionization from the $E,F^1\Sigma_g^+(v)$ state for $v=0-9$ and a photon energy of 10 eV. Black lines: dissociative ionization cross section; red dashed lines: nonresonant contribution.

13). These oscillations are not accidental: they are almost an exact replica of the square of the outerwell vibrational states shown in Fig. 1(b). Indeed, for these outerwell vibrational states, the contribution of resonant processes through intermediate Q_1 or Q_2 doubly excited states is almost negligible. Therefore, direct ionization maps the initial vibrational distribution of internuclear distances onto the repulsive $^2\Sigma_u^+(2p\sigma_u)$ potential of H_2^+ thus yielding a KED spectrum that looks similar to the squared nuclear vibrational wave function. A similar mapping of the initial vibrational wave functions has been observed in H_2 double photoionization [23]. Thus inverting this process can be used to determine the squared nuclear vibrational wave function from the measured KED spectrum. The former analysis does not apply to the inner-well states $v=0$ and 3, and to a lesser extent to $v=6$. For these initial states, photoionization is only possible through the $^2\Sigma_g^+(1s\sigma_g)$ state of H_2^+ (see Fig. 1). Furthermore, as mentioned above, the Q_1 doubly excited states are efficiently populated at this photon energy, thus leading to a KED that is almost entirely due to autoionization. Figure 13 shows indeed that the nonresonant contribution is negligible for $v=0$ and 3. Also the cross section is significantly smaller.

The main conclusions obtained for a photon energy of 10 eV remain approximately valid in the photon energy range 8 to 12 eV. At higher photon energies, contribution of the Q_2 doubly excited states begin to change this picture, especially for the outerwell initial vibrational states.

V. CONCLUSIONS

We have performed a theoretical study of dissociative and nondissociative photoionization of H_2 from the $E,F^1\Sigma_g^+(v,J=0)$ excited state for $v=0-9$ in the photon energy range 3 to 14 eV. The method takes into account both electronic and vibrational degrees of freedom and includes both direct and resonant (through Q_1 and Q_2 doubly excited states) ionization channels as well as the interference between them. Cross sections differential in the energy of the remaining H_2^+ ion or in the proton kinetic energy have been evaluated in the 3–14 eV energy range. We have paid special attention to the case of a photon energy of 6.4 eV corresponding to the wavelength of a ArF excimer laser. Comparison of our results with the available experimental measurements is good. We have shown that contribution of the Q_1 doubly excited states to the measured dissociative ionization cross section is more important than originally believed. At higher photon energies, we have found that, for most initial v's, dissociative ionization is the dominant process.

Very different results are obtained depending on the initial vibrational state. This is the consequence of the double minimum in the potential energy curve of the initial $E,F^1\Sigma_g^+(v,J=0)$ state. For the innerwell vibrational states, photon absorption is only effective in an interval around $R=2$ a.u., while, for the outerwell vibrational states, photon absorption takes place in an interval around $R=4.5$ a.u. This implies that, at a fixed photon energy, very different final states can be reached depending on the initial vibrational state. For instance, at a photon energy of 10 eV, we have found that nonresonant dissociative ionization through the $^2\Sigma_u^+(2p\sigma_u)$ threshold is the dominant process for the outerwell initial states, whereas resonant autoionization through the Q_1 doubly excited states is the dominant one for the innerwell initial states. Thus, by just selecting different initial vibrational states one can induce a variety of ionization processes in H_2 that, in ground state photoionization, would only be possible by strongly varying the photon energy.

ACKNOWLEDGMENTS

Work supported by the DGI (Spain) Projects No. BFM2003-00194 and No. FIS2006-00298, and the European COST action D26/0002/02. We thank the CCC-UAM (Centro de Computación Científica of Universidad Autónoma de Madrid, Spain) for its generous allocation of computer time.

[1] F. Martín, J. Phys. B **32**, R197 (1999).
[2] S. Strathdee and R. Browning, J. Phys. B **12**, 1789 (1979).
[3] C. J. Latimer, J. Geddes, M. A. MacDonald, N. Kouchi, and K. F. Dunn, J. Phys. B **29**, 6113 (1996).
[4] K. Ito, R. I. Hall, and M. Ukai, J. Chem. Phys. **104**, 8449 (1996).
[5] F. Martín *et al.*, Science **315**, 629 (2007).
[6] I. Sánchez and F. Martín, Phys. Rev. Lett. **79**, 1654 (1997).
[7] I. Sánchez and F. Martín, Phys. Rev. Lett. **82**, 3775 (1999).
[8] C. A. de Lange, Int. Rev. Phys. Chem. **20**, 1 (2001).

[9] S. L. Anderson, G. D. Kubiak, and R. N. Zare, Chem. Phys. Lett. **105**, 22 (1984).
[10] E. Xu, A. P. Hickman, R. Kachru, T. Tsuboi, and H. Helm, Phys. Rev. A **40**, 7031 (1989).
[11] W. T. Hill, III, B. P. Turner, S. Yang, J. Zhu, and D. L. Hatten, Phys. Rev. A **43**, 3668 (1991).
[12] S. Yang and W. T. Hill, III, Phys. Rev. A **51**, 2301 (1995).
[13] B. L. G. Bakker, D. H. Parker, and W. J. van der Zande, Phys. Rev. Lett. **86**, 3272 (2001).
[14] H. Rudolph, D. L. Lynch, S. N. Dixit, V. McKoy, and W. M. Huo, J. Chem. Phys. **86**, 1748 (1987).
[15] C. Cornaggia, A. Giusti-Suzor, and C. Jungen, J. Chem. Phys. **87**, 3934 (1987).
[16] K. Wolniewicz and K. Dressler, J. Chem. Phys. **112**, 3689 (1994).
[17] I. Sánchez and F. Martín, J. Chem. Phys. **106**, 7720 (1997b).
[18] I. Sánchez and F. Martín, Phys. Rev. A **57**, 1006 (1998).
[19] H. Bachau, E. Cormier, P. Decleva, J. E. Hansen, and F. Martín, Rep. Prog. Phys. **64**, 1815 (2001).
[20] K. Wolniewicz, K. Szalewicz, and H. J. Monkhorst, J. Chem. Phys. **84**, 3278 (1986).
[21] I. Sánchez and F. Martín, J. Chem. Phys. **110**, 6702 (1999b).
[22] J. L. Dehmer and D. Dill, Phys. Rev. A **18**, 164 (1978).
[23] T. Weber *et al.*, Nature (London) **431**, 437 (2005).